The impact of outgassing on the nano-oxides kinetics of ferritic oxide dispersion strengthened steel

Gabriel Spartacus, Joël Malaplate, Frédéric De Geuser, Denis Sornin, Isabelle Mouton, Raphaëlle Guillou, Alexis Deschamps

The impact of outgazing on the nano-oxides kinetics of ferritic oxide dispersion strengthened steel

Gabriel Spartacus [a, b, *], Joël Malaplate [a], Frédéric De Geuser [c], Denis Sornin [a], Isabelle Mouton [a], Raphaëlle Guillou [a], Alexis Deschamps [c]

[a] Université Paris-Saclay, CEA, Service de Recherches Métallurgiques Appliquées, 91191, Gif-sur-Yvette, France.

[b] (current affiliation) Department of Materials Science and Engineering, KTH Royal Institute of Technology, SE-100 44 Stockholm, Sweden.

[c] Univ. Grenoble Alpes, CNRS, Grenoble INP, SIMAP, F-38000 Grenoble, France.

[*] Corresponding author: spartac@kth.se
+336 22 95 36 97
Gabriel Spartacus
Brinellvägen 23
11428 Stockholm, Sweden

Abstract

Oxide Dispersion Strengthened (ODS) steels are studied for their application in fission and fusion nuclear power plants. These steels are processed by powder metallurgy involving a high energy milling of Fe-Cr with oxides powders, followed by outgazing and hot consolidation. The temperature increase during these last two stages triggers the precipitation of a fine dispersion of nano-oxides. The outgazing stage is generally conducted at temperature between 300 and 800 °C for several hours, which can already trigger the formation of nano-oxides, and thus may have an influence on the final nano-oxide characteristics. In this work we assess the nano-oxides size by Small Angle X-Ray Scattering (SAXS) and get insight on the nano-oxides chemical and structural properties by comparison between SAXS and Atom Probe Tomography (APT) during a thermal treatment at 700 °C for 5 h, simulating the outgazing stage. We show that despite that the nano-oxides slightly grow during the 700 °C heating, the final

properties of the nano-oxides in term of size and number density are extremely close to those where no 700 °C isothermal was applied. Moreover, the growth rate of the nano-oxides is surprisingly higher at 700 °C than 1100 °C. APT and SAXS comparison shows that the nano-oxides do not stabilize in terms of stoichiometry and structure in the studied conditions, and that a small quantity of Al remain in the precipitates during this 700 °C isothermal treatment. Both of these factors could influence the nano-oxides kinetics at low temperature.

Graphical abstract

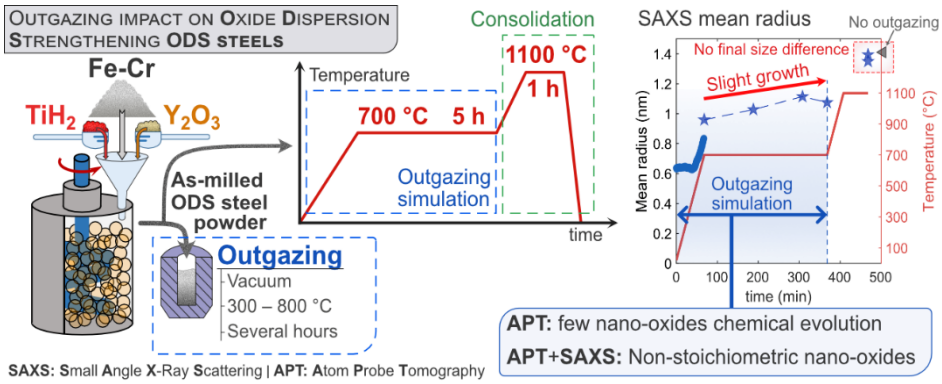

Highlights

- The outgazing shows no influence on the final nano-oxides size and number density.
- No stabilization of the nano-oxides is observed at 700 °C after 5 h isothermal.
- The nano-oxides growth rate is surprisingly higher at 700 °C than at 1100 °C.
- Nano-oxides contains Al on the 700 °C isothermal, which is removed after heating at 1100°C.
- TiC or Ti(C,N) is likely to form after the outgazing, between 700 and 1100 °C.

Keywords:

1. Introduction

Ferritic Oxide Dispersion Strengthened (ODS) steels are studied for their application in fission nuclear power plants as fuel cladding material and in fusion nuclear power plants as structural materials [1,2].

Ferritic ODS steel are composed by a Fe-Cr ferritic matrix providing a good resistance to swelling under neutron irradiation and high corrosion resistance [1,3]. The nano-oxides embedded in the matrix (generally Y-Ti-O oxides) drastically enhance the mechanical properties of the alloy, increasing the creep resistance and yield strength [4,5]. Y-Ti-O nano-oxides of size ~ 3 nm in diameter and high number density (10^{23} to 10^{24}) are finely distributed into the matrix, acting as strong pinning point for Grain Boundaries (GBs) and dislocations up to high temperature due to their outstanding stability and sluggish coarsening up to 1200 – 1300°C [6–8]. The multiple matrix – nano-oxides interfaces also act as efficient He trapping points and mitigate the neutron-induced irradiation [9].

ODS steels are produced by powder metallurgy where an Fe-Cr atomized powder is milled with an Y_2O_3 and a TiH_2 powders into a high energy milling known as Mechanical Alloying (MA). After MA, a quasi-homogeneous distribution of the chemical element can be observed at the micrometric scale while at the nano-scale a very small population of clusters is generally observed [10–14].

The As-MA powder is then generally placed into a sealed low C-steel can and outgassed under vacuum and at temperature varying between 300 °C and 800 °C for several hours, depending on the authors [13,15–17]. The outgazed powder is then compacted during a high temperature process such as hot extrusion or hot isostatic pressing, performed at temperature close to 1100 °C. The nucleation and / or beginning of growth of the nano-oxides had been demonstrated to be as low as 450 °C thanks in-situ synchrotron study of the nano-oxides kinetics [8,18]. Therefore, during the outgazing stage the nano-oxides may evolve, which could have an impact on the final nano-oxides properties. The present work aims at clarifying the potential evolution of nano-oxides during the outgazing stage of the as-MA powder, and its impact on the nano-oxides of the fully consolidated ODS steel, thanks to synchrotron Small Angle X-Ray Scattering (SAXS) and Atom Probe Tomography (APT) measurements.

2. Materials and methods

Fe-14Cr-1W ODS steel was prepared by attrition milling of an atomized powder of Fe-14Cr-1W (with other minor alloying elements) steel powder together with 0.3 wt % of Y_2O_3 and 0.3 wt % of TiO_2. The powder had been Cold Pressed (CP) following the procedure described in reference [12]. After CP the samples are representative of the as-MA stage and more easily observable than in powder form. The chemical composition of this sample (measured) is indicated in the Tab. 1.

Tab. 1: Chemical composition in wt % of the CP sample with the corresponding measurement techniques below.

Fe	Cr	W	Ti	Y	O	C	N	Al

Bal.	13.9 [1]	1.13 [1]	0.27 [2]	0.16 [2]	0.15 [3]	0.031 [4]	0.032 [3]	0.030 [1]

[1] optical emission spectrometry
[2] plasma emission spectrometry
[3] reducing melting thermal conductivity
[4] combustion infrared absorption

The thermal treatment applied on the CP samples was setup as an initial heating ramp from Room Temperature (RT) up to 700 °C with a heating rate of 10 °C/min followed by a 5 h isothermal. Then, another heating ramp from 700 °C to 1100 °C was applied with a similar heating rate (10 °C/min) followed by 1 h isothermal. The 700 °C annealing aimed at simulating the outgazing step at a high temperature where its impact may be important. For comparison, a standard thermal treatment was applied on other CP sample, following a heating ramp from room temperature to 1100°C followed by 1 h isothermal. For this sample, the heating rate was 30 °C/min, which should not influence the final mean radius and number density of the nano-oxides, as demonstrated in a previous work [8].

CP samples were analyzed by SAXS and APT. In-situ synchrotron SAXS measurements were performed during the heating ramp up to 700°C at the European Synchrotron Radiation Facility (ESRF) on the D2AM – BM02 beamline. The X-ray energy was set to 16.829 keV and 17.009 keV in order to analyze the anomalous effect at the Y K-edge (not investigated in the present article but available in [12]). The detector to sample distance was ~ 0.4 m with a 2D XPAD D5 hybrid pixel detector using a 10 sec counting time. Ex-situ SAXS measurements were performed at different stages of the interrupted thermal treatment during the 700°C plateau and subsequent annealing at 1100°C at the Swiss Light Source (SLS) synchrotron of the Paul Scherrer Institute (PSI) on the cSAXS beamline. These measurements were performed at 4.766 keV, using two 2D detectors (Pilatus 2M and Pilatus 300kw) at a sample to detector distance of 2 m and 0.6 m respectively.

For both SAXS measurements, the 2D scattering patterns were azimuthally integrated, background subtracted and the scattering intensity were normalized by solid angle, sample thickness, sample transmission and incident X-Ray beam intensity and reduced into absolute unit thanks to a glassy carbon

secondary standard. Then, the nano-oxides' mean radius and apparent number density (calculated thanks to a hypothesis on the nano-oxides nature) were extracted from the fit between a model assuming a lognormal distribution of spherical precipitates to the experimental data, as explained in more detail on ref [12].

APT analyses were performed at the CEA Saclay for the as-MA and 700°C (without isothermal) stages, measurements on the subsequent stages (700 °C – 5 h and 700 °C – 5 h + 1100 °C – 1 h) were performed at the GPM laboratory of Rouen University. For both measurements, at CEA Saclay and Rouen University, a LEAP 4000X HR instrument equipped with a reflectron in laser mode (60 pJ) were used, operating at 60 K. IVAS 3.6.14 commercial software was used for the 3D reconstruction and calculation of the first Neighbor Distance (1NN) values, necessary for the DIAM algorithm (distribution of isolated atoms for the determination of the matrix composition) applied to extract the matrix composition [19]. In order to calculate the number density of clusters in the APT volumes, the maximum separation method of IVAS have been used to count the clusters present in the volumes. These number of clusters had then be divided by the probed APT volume, calculated thanks to the total number of atoms, the APT instrument detection efficiency (42 %) and the mean atomic volume of BCC Fe. In order to estimates the incertitude of this method, the minimum number of atoms to define a cluster had been varied between 6 and 12. The average values were used to calculate the number density and the standard deviation were given as error bars.

Electron Backscattering Diffraction (EBSD) had been acquired on a JEOL 7001-FLV operating at 20 kV. Orientation maps presented in this article include gran boundaries with misorientation higher than 15°.

3. Results

The orientation maps showinig the granular microstructure of ODS steels at the final stage of the annealing following an heating ramp up to 1100 °C without plateau and with 700 °C plateau for 5 h are displayed in Fig. 1a and Fig. 1b respectively. These micrographs displays a bimodal grain size

distribution, characteristic of consolidated ODS steels. Prior Powder grain Boundaries (PPBs) are also visible as well as some porosities located at some of the PPBs. Those porosities originates from the cold pressing process from which fully dense sample could not be achieved. No clear difference can be noticed from the comparison of the two microstructures.

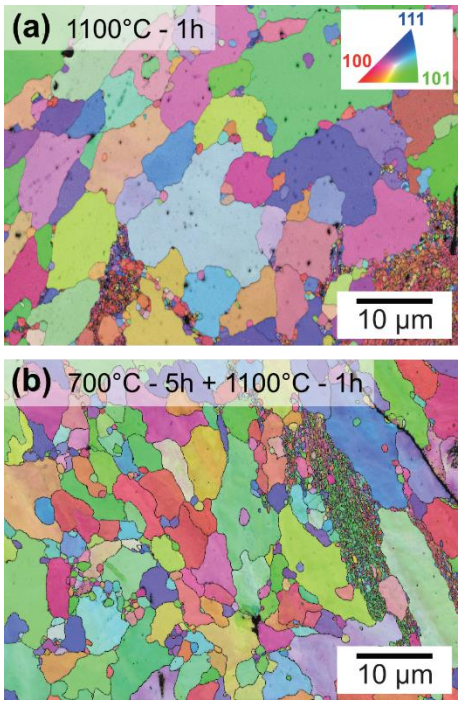

Fig. 1: EBSD orientation mapping of the final stage of the thermal treatment without 700 °C plateau (a), and with 700 °C plateau (b), displaying similar microstructures.

The experimental SAXS intensity curves are shown in Fig. 2, together with the model fitting in continuous lines. Two samples were measured in the condition 700 °C – 5 h + 1100 °C – 1 h and are referenced as (1) and (2) on the figure. Those final steps of annealing can also be compared to the 1100 °C – 1 h condition (without 700 °C plateau) represented in the graph. On these curves, it can be noticed that the precipitates contributions remain very close for all samples at 700 °C, and shift toward lower q-values after reaching 1100 °C, indicating the growth of the nano-oxides. No clear difference can be noticed on the precipitates contribution between the 1100 °C – 1 h and 700 °C – 5 h + 1100 °C – 1 h conditions. A slight difference can be seen on the Porod contribution

(visible at low q-value), which should be linked to difference microstructural differences such as coarse precipitates or porosities.

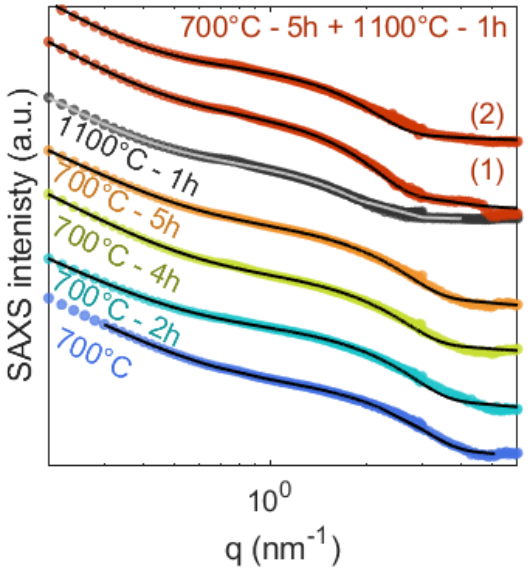

Fig. 2: SAXS intensity curves of the CP specimens displaying similar scattering pattern on the 700 °C plateau.

From the model fitting of the SAXS intensity curves, the evolution of the mean radius of precipitates is extracted and plotted in Fig. 3 as stars, and complemented by the result of in-situ SAXS performed at the ESRF during the heating ramp up to 700 °C. The results from the CP samples that followed a 1100 °C – 1 h thermal treatment (without 700 °C plateau) is given as a grey triangle on the right axis, as comparison point.

A small shift of approximately 0.1 nm is observed between the PSI and ESRF, and was attributed to a potential texture effect highlighted by the PSI experimental setup [12]. The evolution of the nano-oxides size should however not be affected by this artefact that is equivalent on all PSI scattering curves. The experimental data show a moderate increase of the nano-oxides size with the time at 700°C. Even if this increase is small, it remain non-negligible regarding the almost absence of coarsening observed previously at 1100 °C [8]. At the end of the thermal treatment, the nano-oxides mean size are very close

to the value measured on the CP 1100 °C – 1 h without outgazing stage, and in general to those classically achieved in ODS steels with Y-Ti-O nano-oxides [11,13].

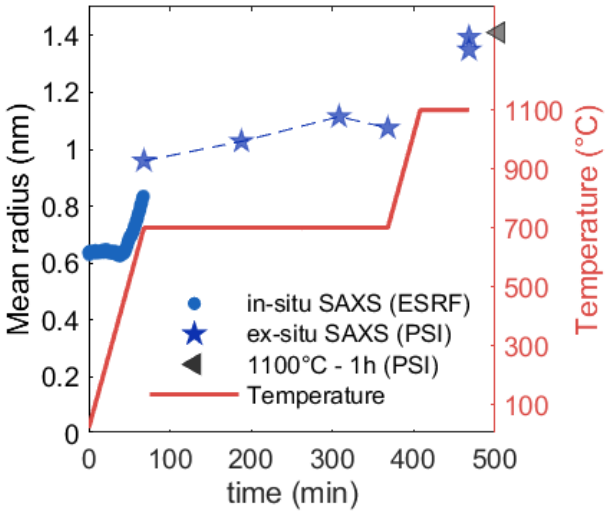

Fig. 3: Evolution of the mean radius of nano-oxides on CP specimens

The APT 3D reconstructions are displayed in Fig. 4. In these reconstructions, the initial as-MA stage demonstrates clusters, as previously found [12]. A decrease of the atoms present in solid solution through the evolution of the thermal treatment is also visible.

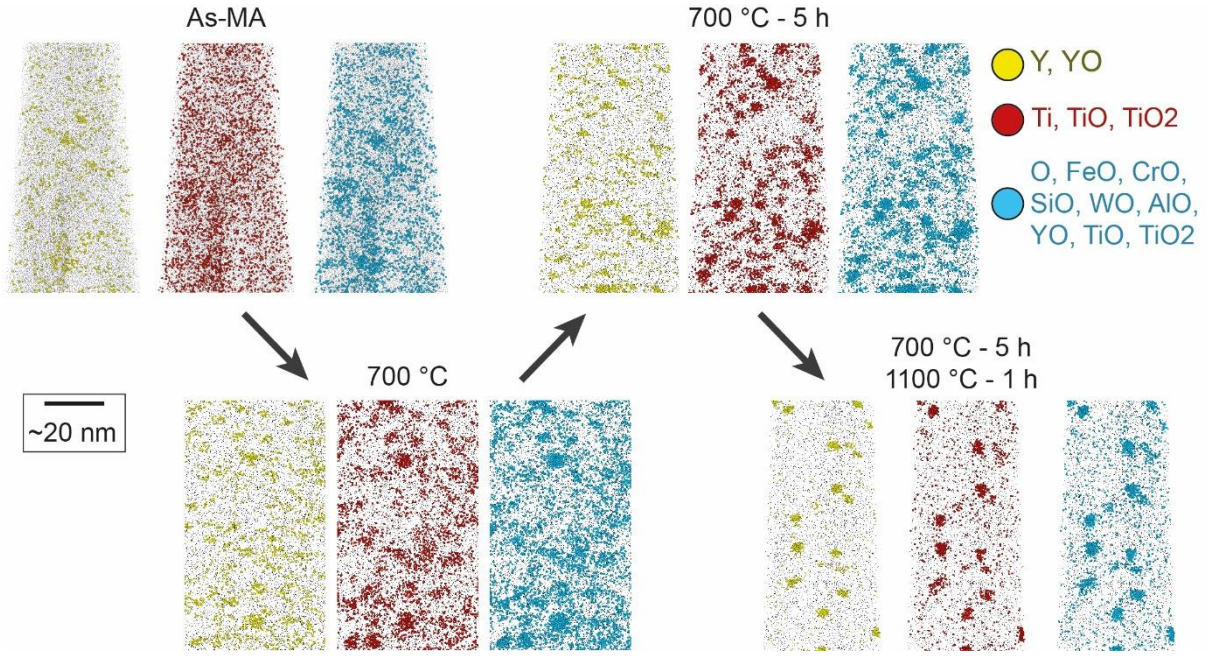

Fig. 4: APT 3D reconstructions showing the Y, Ti and O (with all associated molecular ions) repartition on a ~ 10 nm thick slice at different stages of the thermal treatment.

The matrix composition had been extracted thanks to the DIAM method and display together with the bulk composition (where only the GBs had been removed) in the Fig. 5. This representation leaves us with two areas of interest: the first, in between the bulk and matrix composition curves, related to the amount of atoms present in the nano-oxides. And the second, below the matrix composition curve, related to the amount of atoms present in solid solution. The bulk composition of the Y can be considered as constant all along the thermal treatment, considering the available estimates of the error values. The bulk composition of O seems to decrease at the final stage of annealing, which could be coherent with the formation of coarse oxides (not embedded in the APT volumes due to their low number density), but should be considered with caution as the quantification of O with APT remains uncertain. The bulk composition of Ti clearly decreases between 700 °C – 5 h and 700 °C – 5 h + 1100 °C – 1 h, indicating the formation of coarse Ti-rich precipitates such as Ti(C,N) or Ti-oxides, already identified in this ODS steel grade [20]. The bulk composition of C decreases significantly as well between 700 °C – 5 h and 700 °C – 5 h + 1100 °C – 1 h, which indicates that most of the carbide phases ($M_{23}C_6$, Ti(C,N)…) form after 1100 °C annealing and subsequent cooling. Considering Y, Ti, O, Al and C, the bulk and matrix composition remain fairly constant comparing to the error estimates during the 5 h annealing at 700°C.

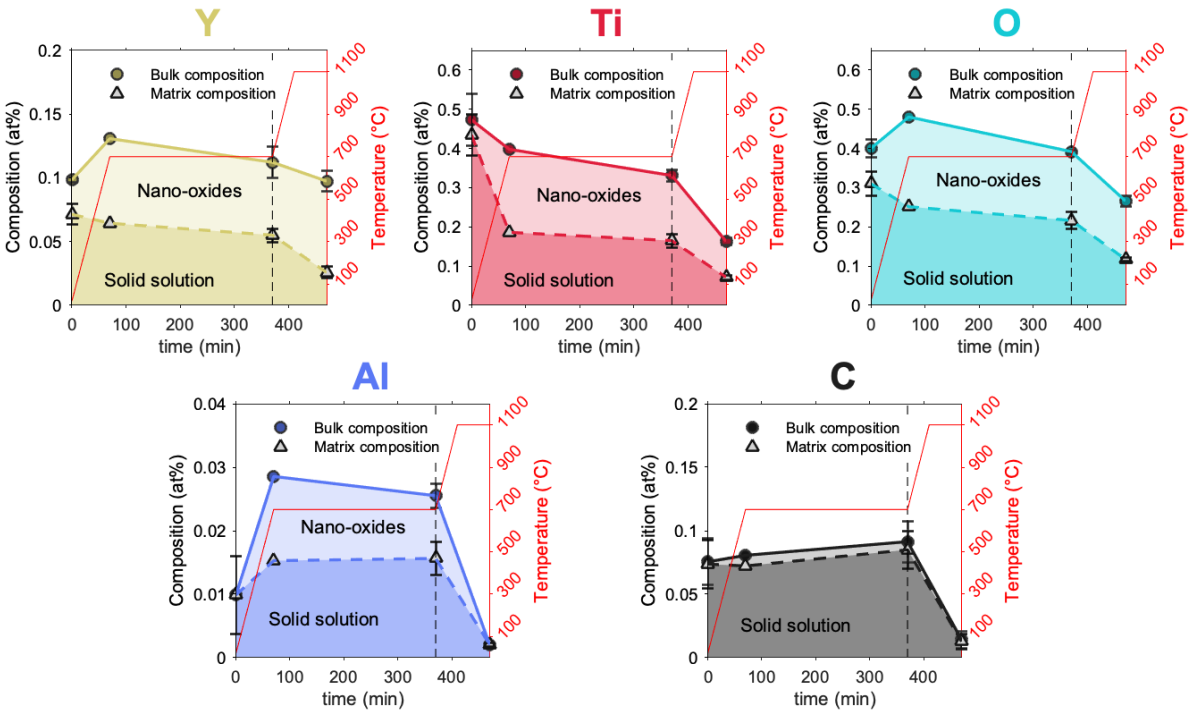

Fig. 5: Evolution of the bulk and matrix composition during the thermal treatment extracted from APT thanks to the DIAM method (for the matrix composition).

The evolution of the number density of nano-oxides is plotted in Fig. 6, and displays both the number density calculated by SAXS, on the assumption that all the nano-oxides are $Y_2Ti_2O_7$, and by APT using the maximum separation method to count the clusters. The average number of clusters used to calculate the number density are given in Tab. 2. Once again, the results from the CP sample in the 1100 °C – 1 h condition is given as a grey triangle, for comparison purpose. As the number density calculated by SAXS is only valid when the hypothesis of $Y_2Ti_2O_7$ nano-oxide is valid, a significant gap between the SAXS and APT data correspond to a stage when the nano-oxides are still far away from the $Y_2Ti_2O_7$ stoichiometry and/or structure. As seen on the graph, this gap (of almost one order of magnitude) exists all along the 700 °C plateau. Moreover, even though this gap slightly decreases with time, a stabilization of the nano-oxides is not likely to occur before a very long annealing at 700 °C. After the 700 °C – 5 h plateau and the subsequent heating at 1100°C for 1 h, the SAXS and APT number density join at a value close to ~ 6.5×10^{23}, which indicates the stabilization of the nano-oxide structure. This value is very

close to that measured in ODS steels without outgazing stage (grey triangle), as well as in classically processed ODS steels [13,21].

Tab. 2: Average (over the varying minimum number of atoms to define a cluster) of the number of clusters identified in each stage, if several APT volumes are available on one stage, the values are summed.

Annealing stage	As-MA	700 °C – 0 h	700 °C – 5 h	700 °C – 5 h + 1100 °C – 1 h
Average number of identified clusters	69	634	334	912

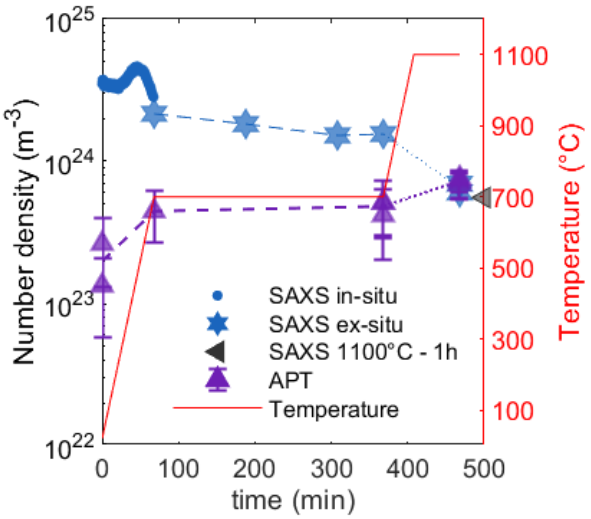

Fig. 6: Evolution of the number density of nano-oxides calculated by SAXS (in blue), based on a precipitates' nature assumption ($Y_2Ti_2O_7$), and measured by APT (in purple triangles).

4. Discussion

During the 700 °C plateau, the mean radius of nano-oxides displays a slight increase (~ 0.1 nm), which interestingly looks more significant than the nano-oxides growth observed at 1100 °C in a previous study [8]. Previous works allow to determine thanks to comparison between SAXS and APT that the nano-oxides structure and stoichiometry should stabilize roughly around 1000 °C [12]. It is also

suggested that this stabilization could lead to the outstanding stability of the nano-oxides as the growth rate of nano-oxides stabilize quickly after this temperature and show almost no coarsening even after 12 h at 1100°C. In our study, the SAXS and APT data comparison clearly shows that a stable stoichiometry and/or structure is not achieved during the 700 °C plateau. Therefore, it is possible that the nano-oxide growth at 700 °C would be linked to this non-stabilized nature of the nano-oxides.

The presence of Al in the nano-oxides at 700°C is another potential explanation for this growth. Indeed, an enrichment of the nano-oxides in Al is observed during the first stages of thermal treatment. Then, during the 700 °C plateau, the Al is very stable and remains inside the nano-oxides. The effect of Al on the nano-oxide kinetics at these small concentrations is still unclear, but at larger concentrations, like in Y-Al-O strengthened ODS steels, the growth and coarsening of nano-oxides is known to be significantly higher [22]. After annealing at 1100 °C, Al cannot be found neither in the nano-oxides nor in the matrix, which is coherent with previous observations made on ODS steel that followed a heating ramp and 1 h isothermal at 1100 °C, without 700 °C isothermal. This absence of Al both in the matrix and in the nano-oxides could be due to the migration of the Al through other features such as precipitates (potentially Y-Al-O, AlN …), GBs, etc. which mechanism seems to require high temperature, as 5 h at 700 °C is clearly not sufficient.

It can be noticed that despite this slight growth of the nano-oxides during the 700 °C annealing, the final nano-oxides size does not seems higher than in an ODS steel that followed a single heating ramp until 1100 °C. Thus, the outgassing step, even performed at relatively high temperature (700 °C) does not seem to have an impact on the final nano-oxides mean size and number density. Moreover, the chemical composition of the matrix at the end of the thermal treatment is also similar to what can be found on an ODS steels that did not withstand a 700 °C isothermal [12].

APT measurements showed that the solid solution of every probed elements remains at a relatively constant and high value throughout the 700°C heat treatment, showing once more that the nano-precipitates are still in their very early stage, with an ill-defined structure, probably distinct from the

pyrochlore phase found after 1100°C annealing. One can estimate that reaching such a stage of precipitation at 700°C only would necessitate a very long time, given the observed kinetics.

The C content remains fairly high after 700 °C – 5h, and drops only at the last stage, indicating that coarse carbides are present in the alloy at the final annealing stage, but not captured in the APT volumes. At 1100°C, $M_{23}C_3$ and M_7C_3 types of carbides (very common in these steels) are not expected to be stable [20]. Moreover, this drop of C bulk composition matches with the drop of Ti bulk composition. Therefore, this event is likely to correspond to the precipitation of a significant amount of TiC or Ti(C, N) precipitates, which have previously being identified in a similar ODS steel grade [20]. The precipitation of these phases therefore happens after the outgazing stage. It can be noted however that the specimens followed a fast cooling after annealing, which could influence the carbide precipitation, for instance, at slower cooling rate, $M_{23}C_6$ may have formed after 700 °C 5 h and reduce the bulk C composition.

5. Conclusion

In this work, we have demonstrated that, even when performed at relatively high temperature (700 °C), the outgassing stage does not modify the final nano-oxides characteristics in terms of size and number density after 1100°C annealing. Moreover, there is little chemical evolution of the nano-oxides during 5h at 700 °C. More specifically, we show that the outgassing process (even at 700 °C for 5 h) is not sufficient to stabilize the stoichiometry and structure of the nano-oxides, which remain far from the pyrochlore structure observed at 1100°C. The required time for a stabilization, if achievable, is very likely to be extremely long. Finally, Aluminum, an common impurity of ODS steels, is found in the nano-oxides at 700 °C and remains all along the 700 °C - 5 h isothermal before leaving the nano-oxides after 1100 °C - 1 h annealing. The formation of TiC or Ti(C,N) had been demonstrated to form at high temperature (between 700 and 1100 °C), after the outgazing stage.

Acknowledgements

For the atom probe tomography measurement the authors acknowledge the French platform METSA as well as the University of Rouen where part of the measurement had been conducted, with the precious help of Bertrand Radiguet and Fabien Cuvilly. We acknowledge Andreas Menzel and the cSAXS beamline team at PSI – SLS synchrotron for the anomalous SAXS measurements at the Ti K-edge and help provided with the data processing. The authors acknowledge Nathalie Boudet, Nils Blanc, Gilbert Chahine and Stephan Arnaud from D2AM-BM02 beamline at the ESRF synchrotron for the in- and ex-situ anomalous SAXS measurement at the Y K-edge. This work received assistance from the "Agence Nationale de la Recherche" program GENESIS referenced as ANR-11-EQPX-0020. This research was founded by the Reactors of 4th Generation (R4G) program of the French Alternative Energies and Atomic Energy Commission (CEA).

References

[1] P. Yvon, M.L. Flem, C. Cabet, J.L. Seran, Structural materials for next generation nuclear systems: Challenges and the path forward, Nuclear Engineering and Design. 294 (2015) 161–169. https://doi.org/10.1016/j.nucengdes.2015.09.015.

[2] S.J. Zinkle, J.L. Boutard, D.T. Hoelzer, A. Kimura, R. Lindau, G.R. Odette, M. Rieth, L. Tan, H. Tanigawa, Development of next generation tempered and ODS reduced activation ferritic/martensitic steels for fusion energy applications, Nuclear Fusion. 57 (2017) 092005. https://doi.org/10.1088/1741-4326/57/9/092005.

[3] T. Tanno, M. Takeuchi, S. Ohtsuka, T. Kaito, Corrosion behavior of ODS steels with several chromium contents in hot nitric acid solutions, Journal of Nuclear Materials. 494 (2017) 219–226. https://doi.org/10.1016/j.jnucmat.2017.07.008.

[4] M. Dadé, J. Malaplate, J. Garnier, F. Barcelo, F. Mompiou, P. Wident, A. Deschamps, Influence of temperature and strain rate on the deformation and damage mechanisms of oxide dispersion

strengthened ferritic steels, Materialia. 4 (2018) 585–594. https://doi.org/10.1016/j.mtla.2018.11.016.

[5] S. Ukai, T. Okuda, M. Fujiwara, T. Kobayashi, S. Mizuta, H. Nakashima, Characterization of High Temperature Creep Properties in Recrystallized 12Cr-ODS Ferritic Steel Claddings, Journal of Nuclear Science and Technology. 39 (2002) 872–879. https://doi.org/10.1080/18811248.2002.9715271.

[6] J. Ribis, M.A. Thual, T. Guilbert, Y. De Carlan, A. Legris, Relaxation path of metastable nanoclusters in oxide dispersion strengthened materials, Journal of Nuclear Materials. 484 (2017) 183–192. https://doi.org/10.1016/j.jnucmat.2016.12.007.

[7] J. Ribis, M.-L. Lescoat, S.Y. Zhong, M.-H. Mathon, Y. De Carlan, Influence of the low interfacial density energy on the coarsening resistivity of the nano-oxide particles in Ti-added ODS material, Journal of Nuclear Materials. 442 (2013) S101–S105. https://doi.org/10.1016/j.jnucmat.2012.10.051.

[8] G. Spartacus, J. Malaplate, F. De Geuser, D. Sornin, A. Gangloff, R. Guillou, A. Deschamps, Nano-oxide precipitation kinetics during the consolidation process of a ferritic oxide dispersion strengthened steel., Scripta Materialia. 188 (2020) 10–15. https://doi.org/10.1016/j.scriptamat.2020.07.003.

[9] T. Stan, Y. Wu, J. Ciston, T. Yamamoto, G.R. Odette, Characterization of polyhedral nano-oxides and helium bubbles in an annealed nanostructured ferritic alloy, Acta Materialia. 183 (2020) 484–492. https://doi.org/10.1016/j.actamat.2019.10.045.

[10] S.W. Kim, T. Shobu, S. Ohtsuka, T. Kaito, M. Inoue, M. Ohnuma, Kinetic approach for growth and coalescence of nano-size oxide particles in 9Cr-ODS steel using high-energy synchrotron radiation X-rays in SPring-8, Materials Transactions. 50 (2009) 917–921. https://doi.org/10.2320/matertrans.MER2008439.

[11] N. Oono, S. Ukai, Precipitation of Oxide Particles in Oxide Dispersion Strengthened (ODS) Ferritic Steels, Materials Transactions. 59 (2018) 1651–1658. https://doi.org/10.2320/matertrans.M2018110.

[12] G. Spartacus, J. Malaplate, F. De Geuser, I. Mouton, D. Sornin, M. Perez, R. Guillou, B. Arnal, E. Rouesne, A. Deschamps, Chemical and structural evolution of nano-oxides from mechanical alloying to consolidated ferritic oxide dispersion strengthened steel, Acta Materialia. 233 (2022) 117992. https://doi.org/10.1016/j.actamat.2022.117992.

[13] M.J. Alinger, G.R. Odette, D.T. Hoelzer, On the role of alloy composition and processing parameters in nanocluster formation and dispersion strengthening in nanostuctured ferritic alloys, Acta Materialia. 57 (2009) 392–406. https://doi.org/10.1016/j.actamat.2008.09.025.

[14] C.A. Williams, P. Unifantowicz, N. Baluc, G.D.W. Smith, E.A. Marquis, The formation and evolution of oxide particles in oxide-dispersion-strengthened ferritic steels during processing, Acta Materialia. 61 (2013) 2219–2235. https://doi.org/10.1016/j.actamat.2012.12.042.

[15] P. Olier, M. Couvrat, C. Cayron, N. Lochet, L. Chaffron, Incidence of mechanical alloying contamination on oxides and carbides formation in ODS ferritic steels, Journal of Nuclear Materials. 442 (2013) S106–S111. https://doi.org/10.1016/j.jnucmat.2013.03.090.

[16] Z. Oksiuta, P. Olier, Y. De Carlan, N. Baluc, Development and characterisation of a new ODS ferritic steel for fusion reactor application, Journal of Nuclear Materials. 393 (2009) 114–119. https://doi.org/10.1016/j.jnucmat.2009.05.013.

[17] P. Unifantowicz, T. Płociński, C.A. Williams, R. Schäublin, N. Baluc, Structure of complex oxide nanoparticles in a Fe-14Cr-2W-0.3Ti-0.3Y2O3ODS RAF steel, Journal of Nuclear Materials. 442 (2013) 158–163. https://doi.org/10.1016/j.jnucmat.2013.04.048.

[18] A. Deschamps, F.D. Geuser, J. Malaplate, D. Sornin, When do oxide precipitates form during consolidation of oxide dispersion strengthened steels?, Journal of Nuclear Materials. 482 (2016) 83–87. https://doi.org/10.1016/j.jnucmat.2016.10.017.

[19] F.D. Geuser, W. Lefebvre, Determination of matrix composition based on solute-solute nearest-neighbor distances in atom probe tomography, Microscopy Research and Technique. 74 (2011) 257–263. https://doi.org/10.1002/jemt.20899.

[20] G. Spartacus, J. Malaplate, D. Menut, C. Toffolon-Masclet, D. Sornin, R. Guillou, A. Gangloff, S. Urvoy, F. De Geuser, A. Deschamps, Characterization of the nature and morphology of coarse precipitation in various oxide dispersion strengthened steels, Materialia. 17 (2021) 101117. https://doi.org/10.1016/j.mtla.2021.101117.

[21] A.J. London, S. Lozano-Perez, M.P. Moody, S. Amirthapandian, B.K. Panigrahi, C.S. Sundar, C.R.M. Grovenor, Quantification of oxide particle composition in model oxide dispersion strengthened steel alloys, Ultramicroscopy. 159 (2015) 360–367. https://doi.org/10.1016/j.ultramic.2015.02.013.

[22] C.P. Massey, S.N. Dryepondt, P.D. Edmondson, M.G. Frith, K.C. Littrell, A. Kini, B. Gault, K.A. Terrani, S.J. Zinkle, Multiscale investigations of nanoprecipitate nucleation, growth, and coarsening in annealed low-Cr oxide dispersion strengthened FeCrAl powder, Acta Materialia. 166 (2019) 1–17. https://doi.org/10.1016/j.actamat.2018.11.062.